

# **Automation of optical inspection in Fermilab**

Evgeny Toropov, TD/SRF  
Dmitri Sergatskov, TD/SRF

TD-11-004

## **INTRODUCTION**

The technology of manufacturing SRF cavities, which are used in ILC and ProjectX experiments, is currently improving. However, cavities may not achieve the performance goals due to the quality of the inner surface. One of the technological processes to explore the inner surface is the optical inspection.

Optical inspection is aimed to find the pits on the surface, which usually correspond to quench locations, and to study their shape and origin. Besides, it provides information on the grain structure and the defects of welding.

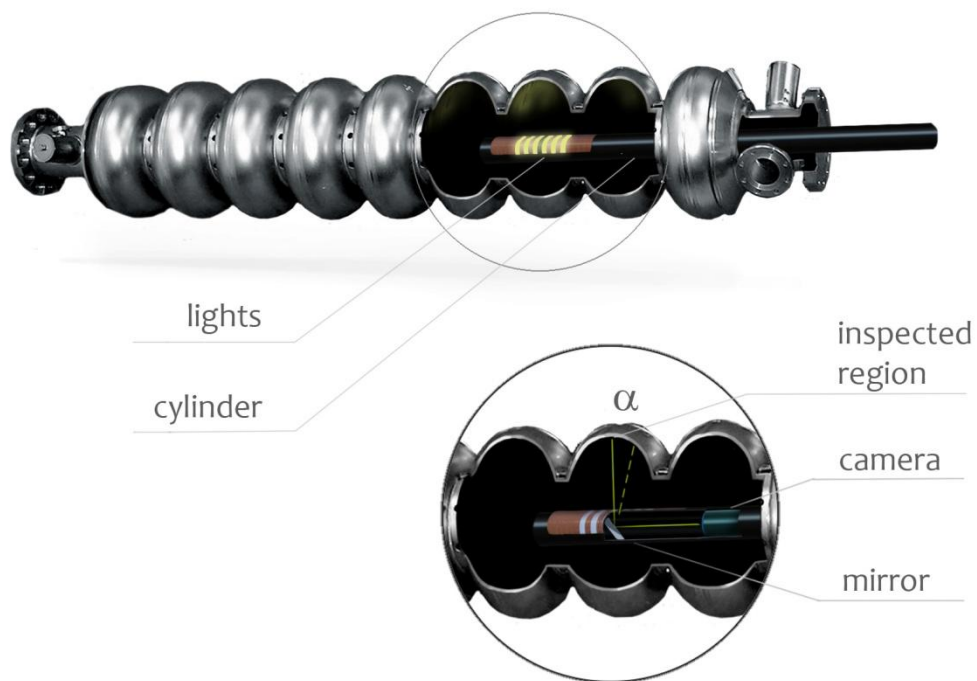
The thorough inspection results in taking several thousands of images and is too difficult to be performed manually. The software has been developed to automate the inspection and to provide a user-friendly interface for working with the inspection system. As a result, the system components included the program set for manual exploring the surface and for the automated inspection.

The main problem of developing the automated system was creating a mechanism to keep the surface in focus. This included two independent components: creating the software for performing autofocusing and applying it efficiently. The methods of autofocusing that can be applied to this case were studied and the suitable algorithm was implemented. The basic components that can be used for developing a similar system and the methods to choose the optimal parameters are described here.

The software was designed to be independent from the hardware characteristics. It can be installed on similar hardware system with no modification and little configuring. The methods described in this paper can also be applied to selecting the inspection system parameters in case the developed software is used on other inspection systems.

## 1. OPTICAL INSPECTION SYSTEM

The optical inspection system is a system that is designed to study the inside surface of a cavity with an optical camera. It consists of a base, a cylinder with the camera, four motors, a rotation angle indicator, and a computer, which is connected to the camera, all the controls and indicators. The cylinder with the camera is mounted onto the base [pic.1]. The cavity is placed onto the base with mechanisms, which differ for different cavities (dressed / not dressed 1.3 GHz, 650 MHz cavities.)



Pic.1

The first motor moves the cavity along the stand. That changes the inspected cell. The second motor changes the angle of rotation – this is accomplished by either rotating the cavity or by rotating the cylinder with the camera.

Refer to the [pic.1] to understand the inner design of the cylinder with the camera. The camera has a constant focal length but it can focus on the surface by moving along the cylinder. The third motor is responsible for moving it. The mirror is adjusted at a certain angle to the cylinder, which can be changed by the fourth motor. This angle affects the angle  $\alpha$ , which will be referred to as the “mirror angle” here. The lights installed at the cylinder are controlled by the separate control box, which in turn can be manipulated programmatically via computer.

The “Omron” indicator is used for the precise measurement of the angle of rotation and can be linked to a cavity or to the cylinder, depending on the system.

All the controls and indicators except the camera are connected to a computer with usb interface. The camera interface differs with the camera type in use. Two Fermilab inspection systems have a IE1394 and a usb interface cameras.

The software for the system manipulation was developed in the LabView environment. Implementation of different mechanisms used in the automated inspection is discussed below.

## 2. AUTOFOCUS

The optical inspection system was designed for automation of inspection process. However, straightforward collecting of images is not possible due to significantly different focal distances for different parts of a cavity.

Therefore, the requirement for the system is the capability to perform automatic focusing, which will be referred to as autofocus. This mechanism is both useful for automated image collection and manual roaming about different cavity parts. Autofocus must be an independent function, taking no parameter inputs and launched by a button click.

Requirements for the autofocus precision vary for two inspection systems at FNAL due to the different focal depth and resolution of the cameras.

	1 <sup>st</sup> system	2 <sup>nd</sup> system (Direct Show mode)
camera name	TELI csf5m7c3l18nr	ArtRay MI900
interface	IE 1394	usb
pixel resolution	1400 × 1000	3488 × 2616
equator field of view (mm)	12.8 × 9.1	7.6 × 5.7
effective resolution (μm)	25 × 15	7.8 × 7.8
effective resolution (pxl)	2.7 × 1.7	3.4 × 3.4
focal depth (mm)	0.2	0.3

Fig.1

“Effective resolution” and “focal depth” were measured with the USAF chart. “Focal depth” was defined as the deviation from the focal distance that causes a significant difference in image sharpness measured by the USAF chart.

Therefore, the goal of the autofocus is to bring an image into focus with the precision of the focal depth. An additional requirement is the operation time minimization: since autofocus

is performed repeatedly, its contribution into the total inspection time is significant and should be minimized.

## 2.1 Autofocus components

For computer focusing is necessarily a process of maximizing some sharpness metrics. The more blurred an image is, the lower the metrics. Metrics is the function of distance to the object, it reaches maximum at the camera focal length. There are several sharpness metrics, which can perform well in different cases. Each of them has parameters to define. Selecting the best one is the first task for developing autofocus.

A metrics does not have to be calculated for the whole image. In fact, it may be advantageous to apply the algorithm to a region of interest on the image – ROI. For small focal depths different image parts are in focus at different focus distances. It is necessary to choose what image part to focus on.

Another component is the mechanism of reaching the peak of the chosen metrics. Mechanisms may differ by the quality, robustness and time. Two algorithms were implemented and discussed here.

Other parameters include lighting conditions and color channel to be used when transforming image to monochrome.

## 2.2 Metrics

Computer regards the process of focusing as maximizing a sharpness metrics for different distances to an object. This metrics is a characteristic of a monochrome image. An example of the metrics is the size of a JPEG file – the more details on a picture the larger its size.

In [1] more than 20 metrics were analyzed and sorted according to several criteria. We chose three successful ones to compare:

### 1. Absolute gradient

$$F_{abs\_grad} = \sum_x \sum_y |i(x+1, y) - i(x, y)|$$

where  $|i(x+1, y) - i(x, y)| > \theta$ ,

$i(x, y)$  is the intensity of pixel  $(x, y)$ ,

$\theta$  is the threshold parameter

2. Brenner gradient

$$F_{Brenner} = \sum_x \sum_y (i(x+2, y) - i(x, y))^2$$

where  $(i(x+2, y) - i(x, y))^2 > \theta$

3. Variance

$$F_{Variance} = \frac{1}{Height \cdot Width} \sum_x \sum_y (i(x, y) - \mu)^2$$

where  $\mu$  is the mean intensity of an image

Extending two of these metrics to more parameters resulted in two more metrics:

4. Extended gradient

$$F_{abs\_grad} = \sum_x \sum_y (dif_{1;0}(x, y) + \dots + dif_{2;2}(x, y) + \dots + \text{any set of summands})$$

where  $dif_{j;k}(x, y) = |i(x+j, y+k) - i(x, y)|$ ,

5. Local variance

$$F_{Variance} = \frac{1}{Height \cdot Width} \sum_x \sum_y |i(x, y) - \mu_r(x, y)|$$

where

$$|i(x, y) - \mu_r(x, y)| > \theta$$

$\mu_r(x, y)$  is the mean intensity in the square with the center in  $(x, y)$  and with  $2r$  side  
 $r$  will be referred to as radius

Each of 5 metrics has its own parameter set. Besides, we compressed the image by the factor of  $\omega$  (integer) to reduce the noise level and to increase the sharpness.

Metrics	Parameters
absolute gradient	downsampling factor $\omega$ , threshold $\theta$
Brenner gradient	$\omega$ , $\theta$
variance	$\omega$
extended gradient	$\omega$ , $\theta$ , set of summands
local variance	$\omega$ , $\theta$ , radius $r$

### 2.2.1 Ranking methodology

Focus function is a dependency of a sharpness metrics on distance from the camera to an object. There are several requirements for a focus function:

- 1) The function maximum should be unbiased with the precision described above (accuracy)
- 2) The function should have a peak sharp enough to enable this precision to be achieved (peak width)
- 3) At the same time, the function should not equal zero too close to the maximum. Otherwise, it may be difficult to find the non-zero area (shoulders width)
- 4) Metrics value at  $x = \pm\infty$  should be small (background). It is important for the fitting algorithm, which is described below
- 5) Noise should not create many local maximums (noise level)

Each of these five requirements can be described numerically. Consider a typical plot of a normalized focus function [Fig. 2]. The difference between the function maximum and the real focal distance (mm) corresponds to the “accuracy”. The width (in mm) of the peak at  $y = 2/3$  is the “peak width” and the width (in mm) of the peak at  $y = 1/5$  is the “shoulders width”. The sum of function values at the minimum and maximum recorded distances ( $y(x_{\min}) + y(x_{\max})$ ) is the “background”. Finally, the percent of points where the focus function is not increasing for  $x < 0$  and not decreasing for  $x > 0$  is considered as the “noise level”.

The set of criteria we used does not match the one described in [1]. The difference is caused by different typical curve shapes and different requirements. For example, we use the “background” criterion due to its role for successful usage of one of the peak-reaching algorithm (see *Optimization* below).

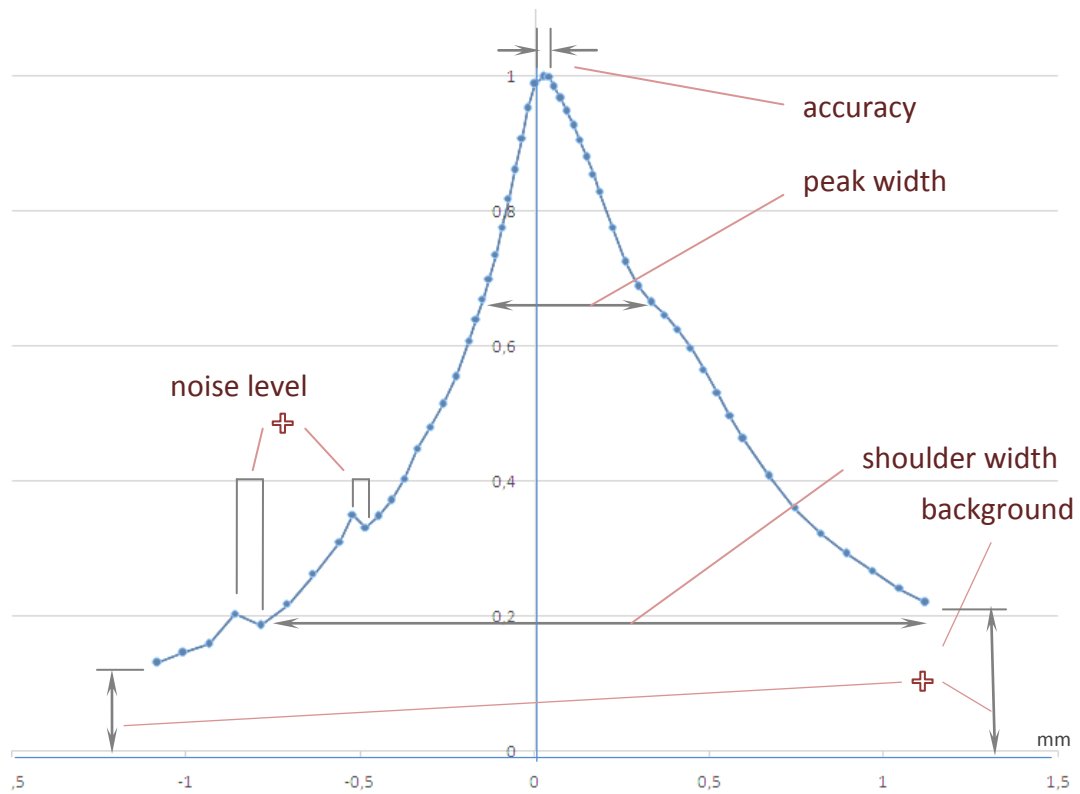


Fig. 2

The focus function is considered to succeed on a certain inspected area if it meets all the criteria below. The parameters are defined beforehand and may be different for different inspection systems.

	Criteria	Parameters 1 <sup>st</sup> system	Parameters 2 <sup>nd</sup> system
1.	"accuracy" < accuracy0	0.01	0.05 mm
2.	"peak width" < peak_width0	0.7 mm	0.7 mm
3.	"shoulders width" > shoulders_width0	0.3 mm	0.3 mm
4.	"background" < background0	0.5	0.5
5.	"noise level" < noise_level0	20%	20%

Fig. 3

The problem is to fulfill all the five requirements for a focus function. To solve it, it is necessary to choose the optimal combination trying different metrics and varying parameters.

The plots below demonstrate how changing metrics parameters influence the focus function for a typical image on the 2<sup>nd</sup> inspection system. The focus functions are normalized.

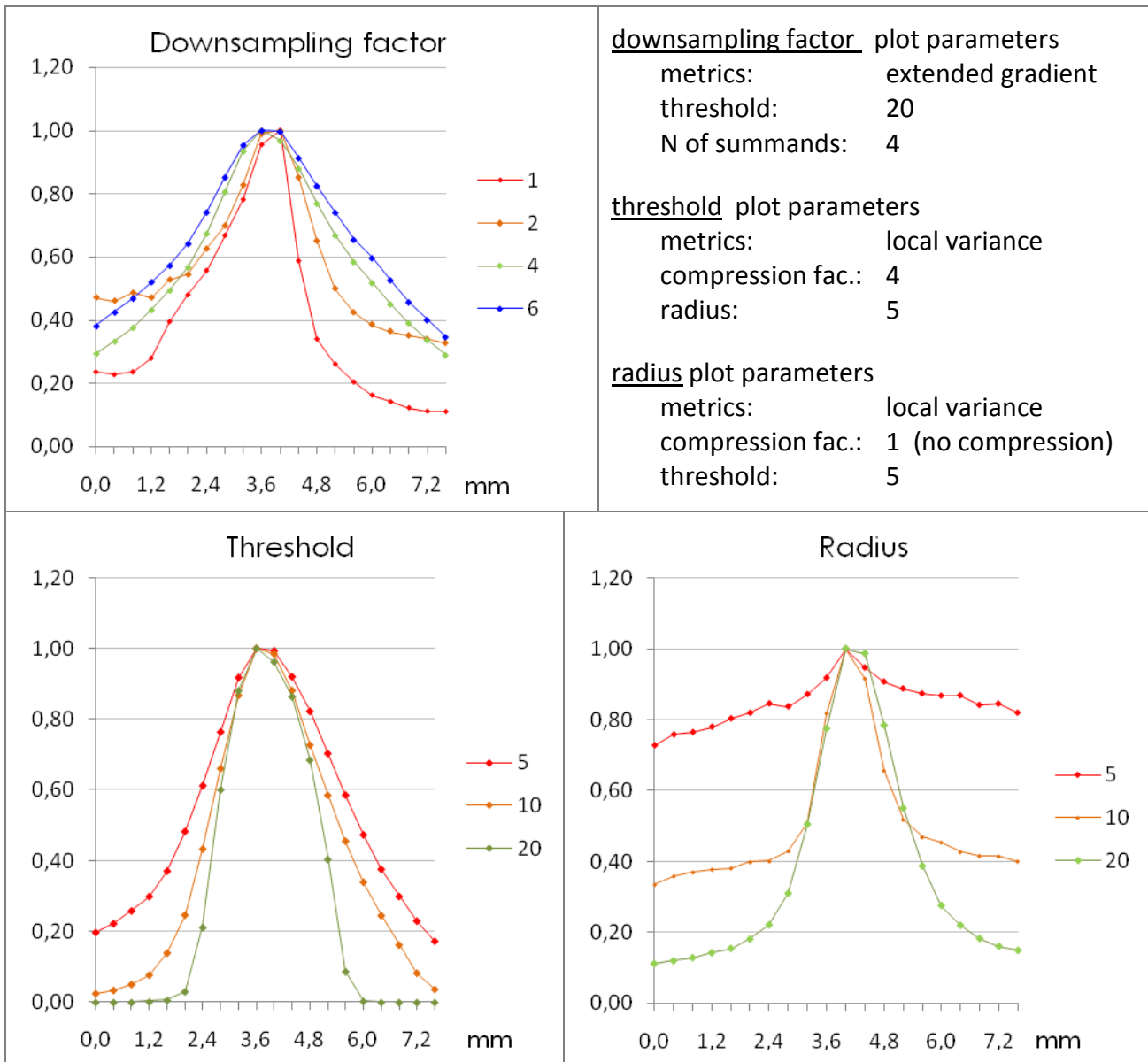
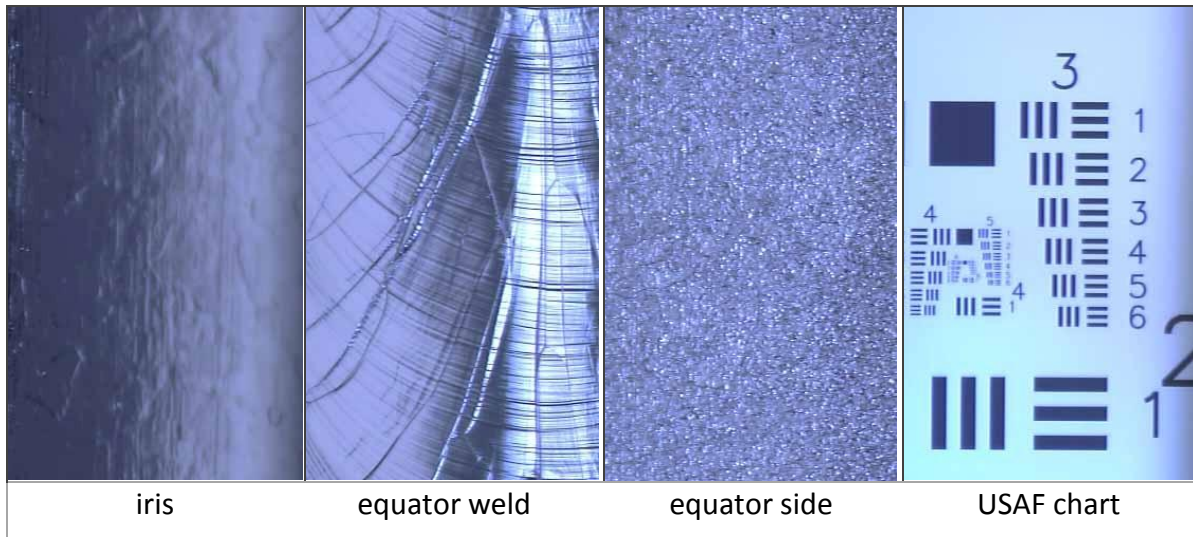


Fig. 4

From the threshold plot you can see that a high threshold can decrease the noise influence – the more the threshold is the sharper is the peak. However, in accordance to requirement (3), a high threshold should be avoided, since it sharpens the peak and narrows the non-zero part of the plot. Hence, it is more difficult to find the hill starting even from near the peak.

Two of the metrics – “extended gradient” and “local variance” – give the best results. To compare them and to choose the best parameters configuration we explored four different sample areas – an iris, an equator weld, an area to the side of equator weld and the USAF resolution test chart [Pic. 2].

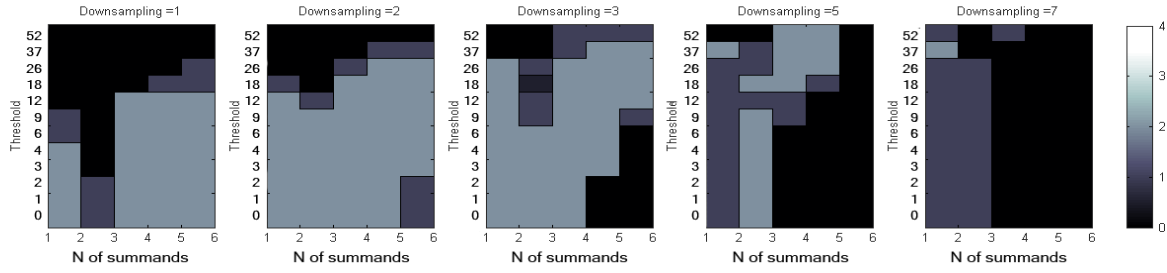


Pic. 2

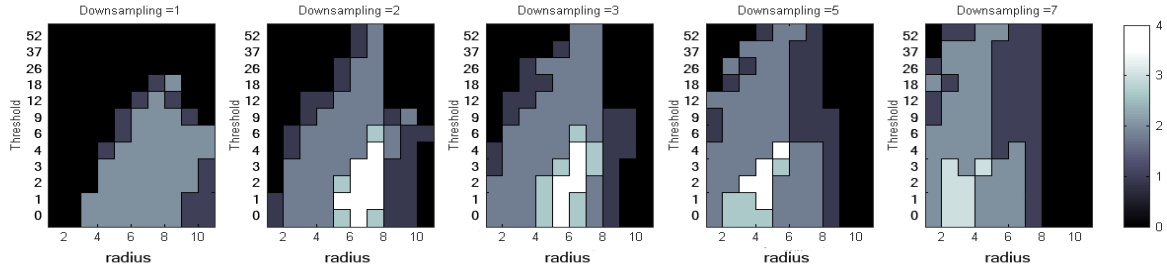
Every specific metrics configuration (metrics, downsampling factor, radius/N summands, threshold) succeeded on different number of these samples (from 0 to 4). The dependency of the number of successes on metrics configuration is shown in the picture below. The black area on the plots corresponds to the metrics failure on all the samples, the white – to the metrics success on all the samples.

# 1<sup>st</sup> system

## Extended gradient

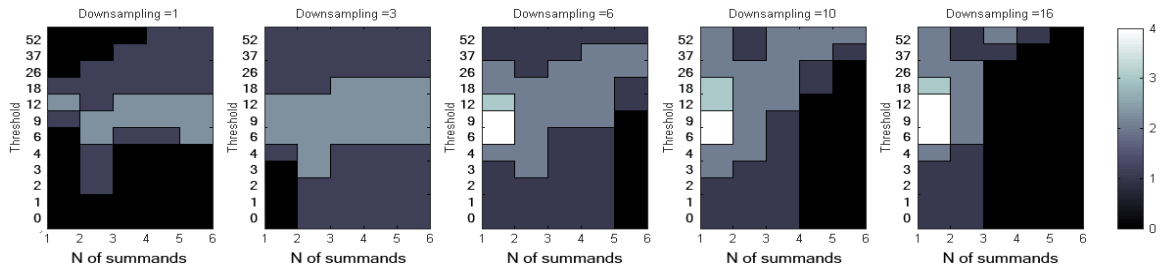


## Local variance



# 2<sup>nd</sup> system

## Extended gradient



## Local variance

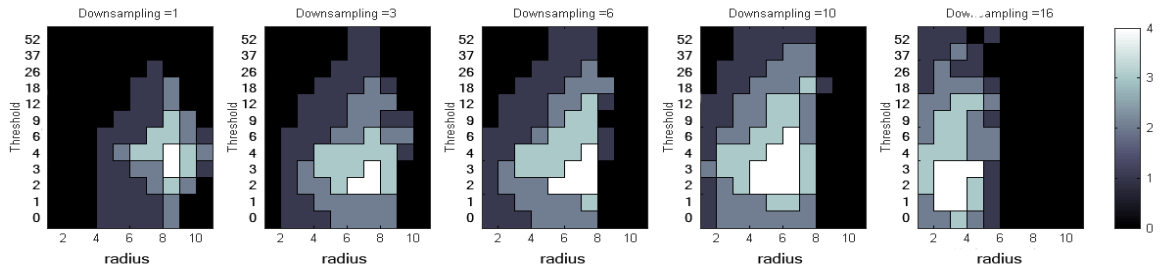


Fig. 5

The “local variance” exhibited a better overall performance than the “extended gradient” on these samples. First of all, it succeeded a greater overall number of times. Besides, a slight shift of parameters from the best configuration does not dramatically affect the performance.

You can also notice that the second system generally needs a higher downsampling factor than the first system to succeed on a greater number of samples. The reason is the low camera effective resolution (in pixels) of the second system [Fig.1].

The optimal metrics for two systems were eventually selected:

	1 <sup>st</sup> system	2 <sup>nd</sup> system
metrics	local variance	local variance
downsampling	2	8
radius	6	5
threshold	2	3

Fig. 6

### 2.3 ROI

A part of an image to apply a metrics to has to be chosen. One approach for choosing ROI is to fix the size of the rectangle and adjust its position on an image. This approach gives better results in different situations and was finally chosen.

The size of the ROI is defined mostly by the focal depth of a camera – the lower the camera focal depth the less part of an image is in focus. Another factor is the lighting conditions: in poor lighting a larger ROI can accumulate more information. In this case, the 1<sup>st</sup> inspection system ROI was chosen as 20% × 20% of image, the 2<sup>nd</sup> system ROI – as 50% × 80% of image.

Next, it is necessary to choose the center of the rectangle. Some criterion must be used for making a decision. It should consider how detailed and how bright the part of an image is. Detailed areas are evidently good for focusing and brighter areas have less noise. Detailed and, at the same time, bright areas give more information to a user and, therefore, should be in focus.

The brightness of an area is well described by the mean intensity, the number of details – by one of the focus metrics. However, every focus metrics is usually a linear function on brightness – the brighter an area is, the more detailed it would appear to the metrics. This can

cause wrong decisions – an over-lighted area with no details would be preferable to a much-detailed but dark area. Therefore, the focus metrics should be normalized on mean intensity.

$$NormM = \frac{M}{I}$$

$NormM$  can also be misleading if two equally detailed areas, a bright and a dark one, are compared.  $NormM$  makes no distinction between them. At the same time, the brighter one is preferable.

We reached the compromise with the final metrics:

$$NormM \times \sqrt{I} = \frac{M}{\sqrt{I}} \rightarrow \max$$

This metrics proved to work well in practice for choosing ROI.

To sum up, to chose the ROI we choose a rectangle of the predefined size (set beforehand as a percentage of the original image). The rectangle must correspond to the maximum value of  $M/\sqrt{I}$ , where  $M$  is the metrics used for focusing and  $I$  is the overall intensity calculated for this rectangle.

## 2.4 Optimization

The motor responsible for the distance to an object is used during reaching the focused position. The motor we use has the accuracy of 0.02-0.04 mm. Besides, it is necessary to wait some time before taking a snapshot; otherwise, an image may be blurred. This time differs from 1 sec. to 1.5 sec. for the 1<sup>st</sup> and the 2<sup>nd</sup> inspection systems.

In this section we will first discuss how the maximum metrics value can be achieved – at the start point the function values for different focal lengths are not known. Hence, it is necessary to take several function value samples and calculate the maximum value accordingly.

A separate problem arises in situations when the algorithm starts far from focused position. The focus function values there are below the metrics noise level. An algorithm is needed to decide on where to look for a maximum in poor conditions.

Finally, it is desirable to avoid a time-consuming procedure of focusing when possible: 15-25% of images are actually focused at the start. Therefore, before autofocusing it is necessary to check whether an image is focused.

The diagram below describes the autofocus algorithm. Positive and negative output results correspond to the success and failure in finding a focused image. A mechanism must be implemented to process negative outcomes. Different options will be discussed in the *Focusing issues* section.

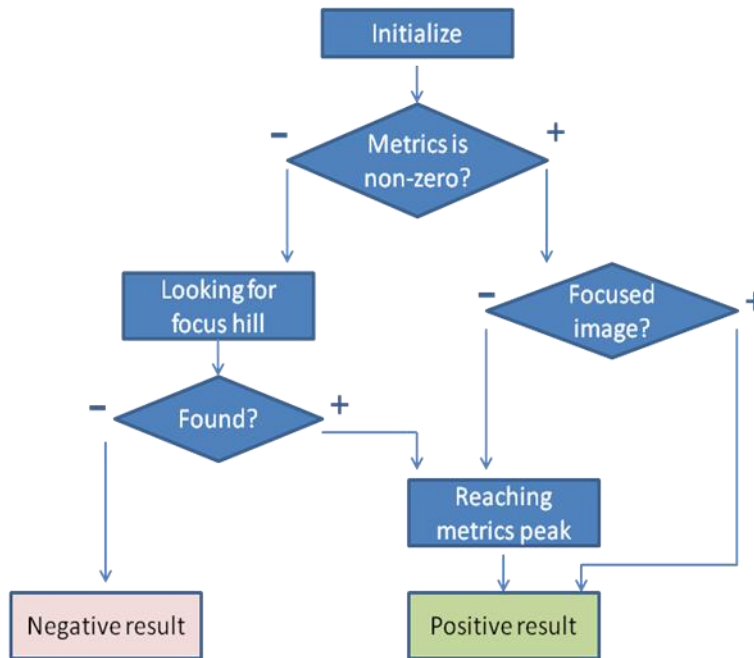
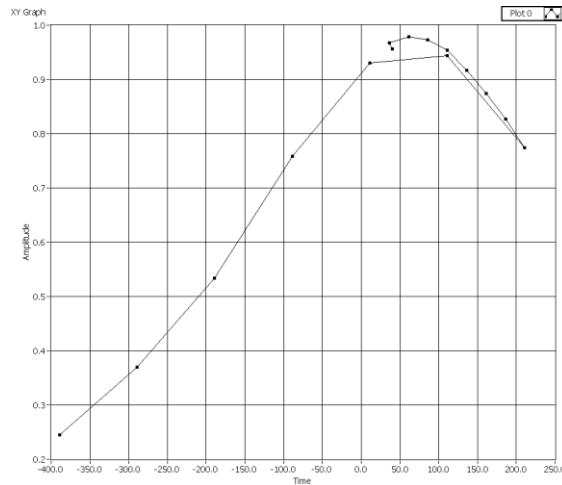


Fig. 7

#### 2.4.1 Hill-climbing

The first and the simplest way to reach the peak is the “hill-climbing” algorithm [2].

- 1) Choose the direction up the slope
- 2) Go in certain step until you cross the maximum
- 3) Repeat “climbing” (2) with finer steps in the opposite direction
- 4) Go to the maximum position



**Fig. 8**

We used two iterations of the climbing with step lengths 0.15 mm and 0.05 mm on the 1<sup>st</sup> system. The 0.05 mm accuracy usually can be achieved.

The major disadvantage of this approach is the low robustness to any outbursts. The decision is made on every step on whether the maximum is met. Therefore, the input on every step must be very accurate. This is especially true near the maximum, where the metrics changes insignificantly. That leads to the second disadvantage of the method – long delay times before taking snapshots and, consequently, long time to focus (see the table below).

Advanced techniques of hill-climbing search such as the adaptive-size step climbing [3] were not selected as well due the high robustness to noise. The noise can be as high as 30% of the signal for non-reflective cavities.

### 2.4.2 Fitting

The second method we implemented is based on the idea that for a well-chosen metrics the focus function is always bell-shaped and, therefore, can be approximated by the gauss function:

$$Gauss(x) = y_0 \times \frac{1}{2\pi\sigma} \exp\left(-\frac{(x-x_0)^2}{2\sigma^2}\right) \quad \text{where } x_0, y_0, \sigma \text{ are parameters}$$

The algorithm we developed aims at taking several metrics samples from both side of the peak. It operates in six steps:

- 1) Choose the direction up the slope

- 2) Go with a certain *step* until you cross the maximum
- 3) Go in the same direction with the same step down the slope until function values are less than *percent* of the maximum recorded value
- 4) Go to the initial position; from that point down the slope until function values are less than *percent* of the maximum recorded value
- 5) Make gauss fitting using all the collected information
- 6) Go to the maximum of the gauss function

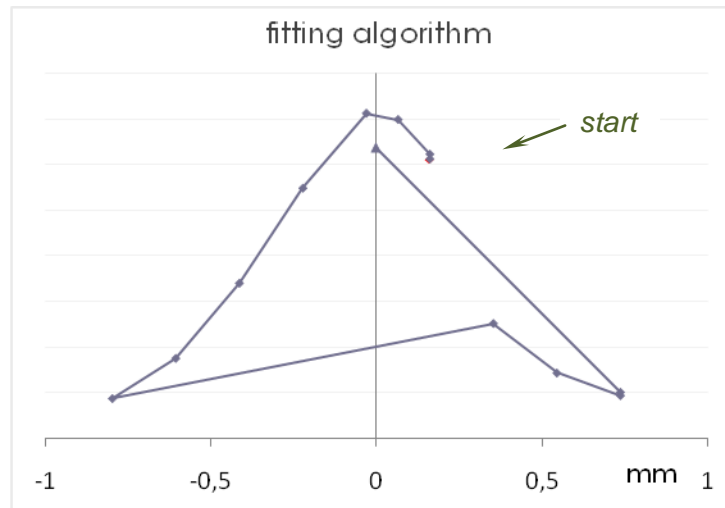


Fig. 9

The input parameters are *step* and *percent*. We used  $step=0.2\text{ mm}$  and  $percent=30\%$  for the 1<sup>st</sup> system.

The gauss function can be well approximated with only 5-6 values of focus function. Besides, approximation outcome is robust to outbursts and noise so the accuracy of the metrics samples does not need to be high. That allowed us to use shorter delay time before taking snapshots (0.1 sec). However, the shorter delay time is partially compensated by the higher number of images to be taken.

The fitting method always takes several images on both sides of the maximum value. This results in good performance in extremely low-signal cases. If the focus function is far from the bell-shaped because of the noise, the fitting algorithm still returns a value close to the maximum [Fig. 10]

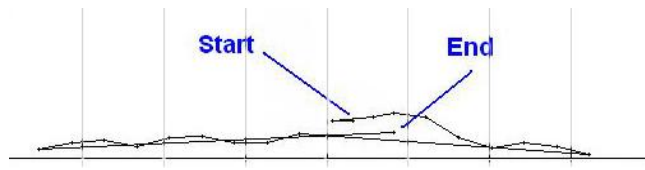


Fig. 10

The comparison of the algorithms for the 1<sup>st</sup> inspection system indicates that the gauss-fitting method is advantageous:

	hill-climbing	gauss-fitting
parameters	$\overrightarrow{steps} = \begin{pmatrix} 0.15 \text{ mm} \\ 0.05 \text{ mm} \end{pmatrix}$	$step = 0.2 \text{ mm}$ $percent = 30\%$
accuracy	0.05 mm	0.05 mm
average time	15 sec.	10 sec.
resistance to fluctuations	low	high

Fig. 11

### 2.4.3 Poor conditions

It is only close to the focal distance that a metrics value is non-zero and exceeds the noise level. However, if the autofocus is launched far from the focal distance, an algorithm is needed to look for a region of non-zero, above-noise-level values of focus function. This region will be referred to as the “focus hill”.

There may be different approaches to manage poor initial conditions. The one we implemented looks for the focus hill within a specified *interval*:

1. Go in the negative direction with a certain *step* until finding the focus hill or reaching the lower *interval* limit
2. If the focus hill is found start autofocusing  
Otherwise go to the initial position; then in the positive direction with the same *step* until finding the focus hill or reaching the upper *interval* limit
3. If the focus hill is found start autofocusing  
Otherwise go to initial position and return the negative output result

#### 2.4.4 Initial check for focus

For the reason of saving time autofocusing is performed only once for several angles during the automated inspection. However, the surface is still likely to remain in focus when a new autofocusing is scheduled. The autofocus procedure is time-consuming even if it starts from a focused image. Therefore, a check at the beginning of autofocus was implemented:

1. Make a single *step* in minus direction
2. If the initial position metrics value was greater, make double *step* in plus direction
3. If the initial position metrics value was greater than the values on both sides, give the positive output result

If the check result is positive the autofocus is considered to be completed.

### 3 INSPECTION ALGORITHM

We used three variables that describe the region of the surface that is being inspected at the moment: the cell number  $x$ , the angle of rotation  $y$ , and the angle of the mirror  $z$ .

The cell number  $x$  takes discrete values. Integer values from 1 to 9 correspond to equator numbers, values from 0.5 to 8.5 – to iris numbers. A typical inspection covers all the equators and irises though a user can select the numbers of cells to inspect.

The rotation variable  $y$  can take discrete values from interval  $[0; y_{\max}]$  where  $y_{\max}$  is preset. The whole interval  $[0; y_{\max}]$  corresponds to 360 degrees of the actual rotation angle.  $y_{\max}$  is chosen so that the images intersection is about 30%.

Mirror angle variable  $z$  changes from  $-z_{\max}$  to  $z_{\max}$ . Depending on the number of the images  $num_z$  per one  $y$ ,  $z_{\max}$  can be an integer or not:

$$\begin{aligned} num_z = 1 \quad z_{\max} = 0 \quad z \in \{0\} \\ num_z = 2 \quad z_{\max} = 0.5 \quad z \in \{-0.5; 0.5\} \\ num_z = 3 \quad z_{\max} = 1 \quad z \in \{-1; 0; 1\} \\ \dots \end{aligned}$$

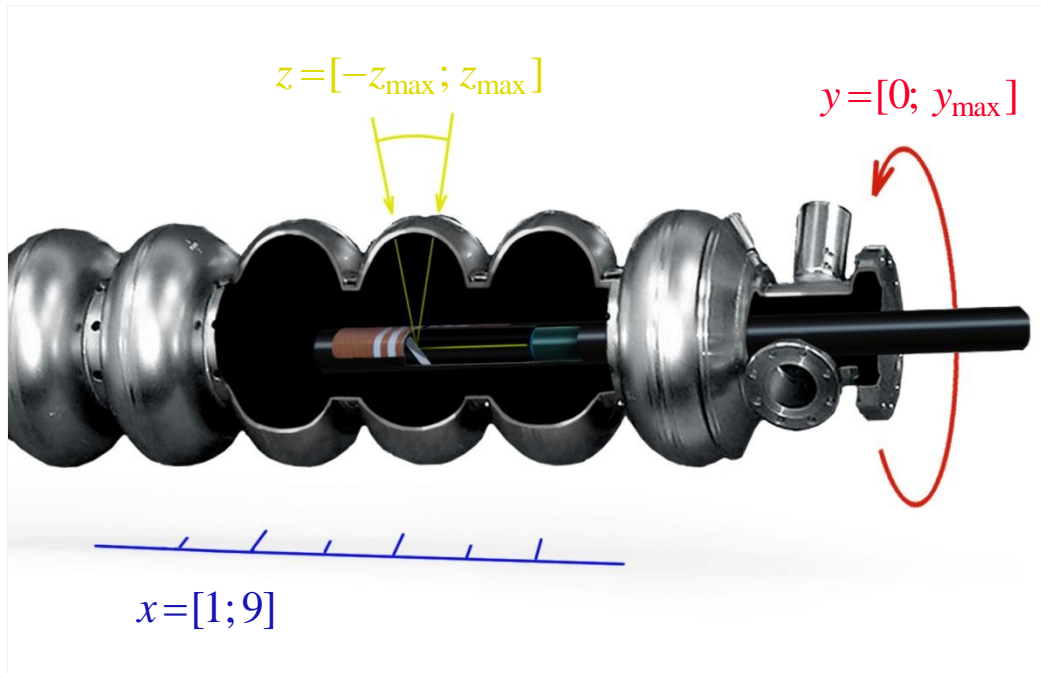
$num_z$  is set so that the range  $[-z_{\max}; z_{\max}]$  covers all the region of interest on an equator or an iris and images have the same 30% intersection.  $num_z$  is different for

equators and irises and for two inspection systems in Fermilab. For the both systems  $num_z = 1$  for irises.

We set the following sequence of the inspection process: first, all the necessary equators are inspected, after that, all the irises. Within one cell all the angles  $y$  are inspected. The value of  $z$  changes within the same angle  $y$  [Pic. 3].

It is preferable to put the  $z$  cycle inside the  $y$  cycle and, therefore to change  $z$  variable for every  $y$  value because, first of all, changing the angle of the mirror requires less relaxation time before a snapshot than rotating cavity does. Besides, if during the post-processing images are stitched together there is no shift between neighbor images.

The overall number of collected images is 2460 and 5560 for the 1<sup>st</sup> and the 2<sup>nd</sup> systems respectively.



Pic. 3

#### 4 FOCUSING ISSUES

The focal distance changes during the inspection. There are several reasons for that. There is an impact of an inspection system: first, a cavity is positioned with some minor angle to the horizontal plane. Second, if changing the  $y$  angle is achieved by rotating the cylinder with the camera, the focal distance differs during the rotation

because the cylinder is not precisely centered. A cavity itself may be slightly arched. Moreover, equators and irises may be wavy.

Exploring the shape of a cavity using the information on focal distance as well as creating an algorithm to efficiently gather and use this information during an inspection in order to keep the surface in focus is discussed below.

#### 4.1 Cavity shape

The information about focal distances can be used to find the significant deviations of the shape of a cavity. The method is based on the fact that the focal length corresponds to the distance between the camera and an explored region. This research was conducted for the 1<sup>st</sup> Fermilab inspection system [4].

The focal length information was collected for different cells and different angles – autofocus was performed 8 times for every iris of the cavity [Fig. 12]. These measurements were made 5 times to reduce the statistical error.

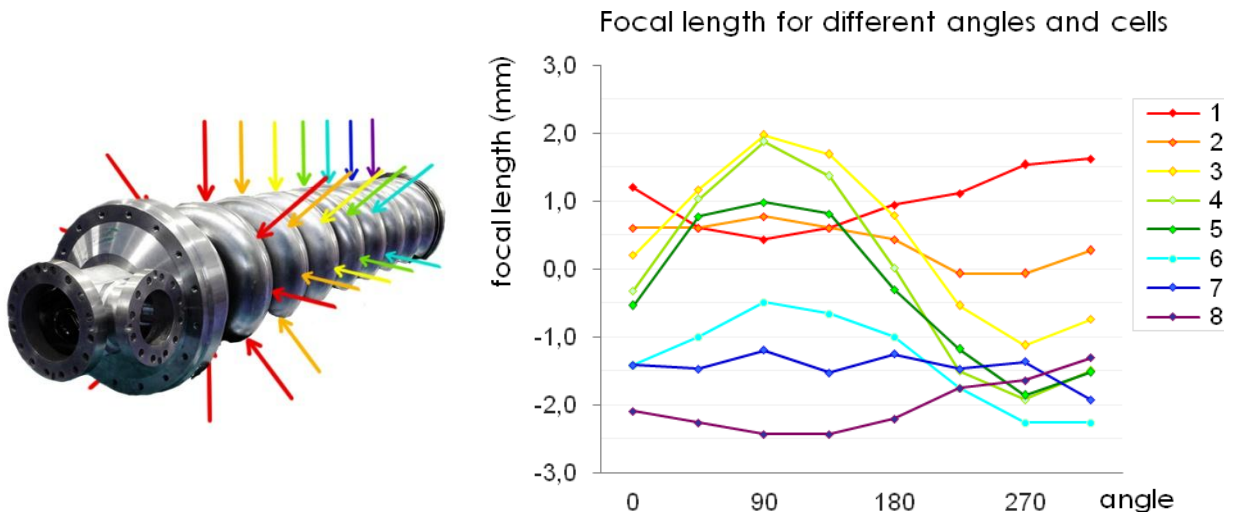


Fig. 12

It can be seen that these plots, which correspond to 8 irises, can be approximated by the sinus function.

$$y(x) = \text{offset} + \text{amplitude} \times \sin(x + \varphi)$$

*Offset*, *amplitude* and *phase* are the functions of the iris number. Below is the plot for *offset(cell)* and *amplitude(cell)*.

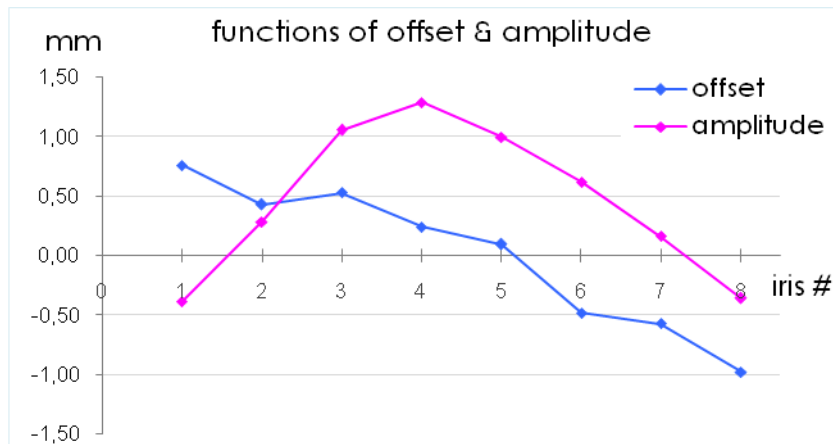
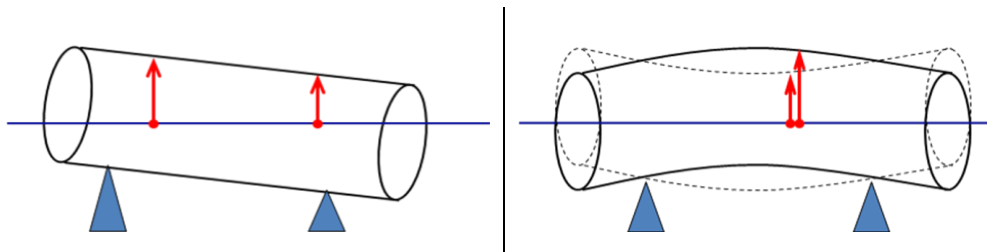


Fig. 13

The *offset* corresponds to the average distance between the cylinder with the camera and the surface. However, the differences in the *offset* are not caused by the differences in the cells radius.



Pic. 4

In the 1<sup>st</sup> system it is the cavity that rotates, not the cylinder. Hence, it is the displacement of a cell center which defines the *offset*. Since the cavity position is not precisely horizontal, the *offset* is a linear function on the cell number. Harmonics *amplitude* differs due to the arc-shape of the cavity. Its value is defined by the cell number. The rollers supported the second and the eighth cells of the examined cavity. That means that the irises which were further from the second and the eighth equators are likely to have a higher *amplitude* value [Fig. 13]. In the linear approximation the shape of the cavity matches the plot of *amplitude*.

The results of the analysis performed for equators of different cavities are exhibited on Fig. 14. The vertical axis is in mm.

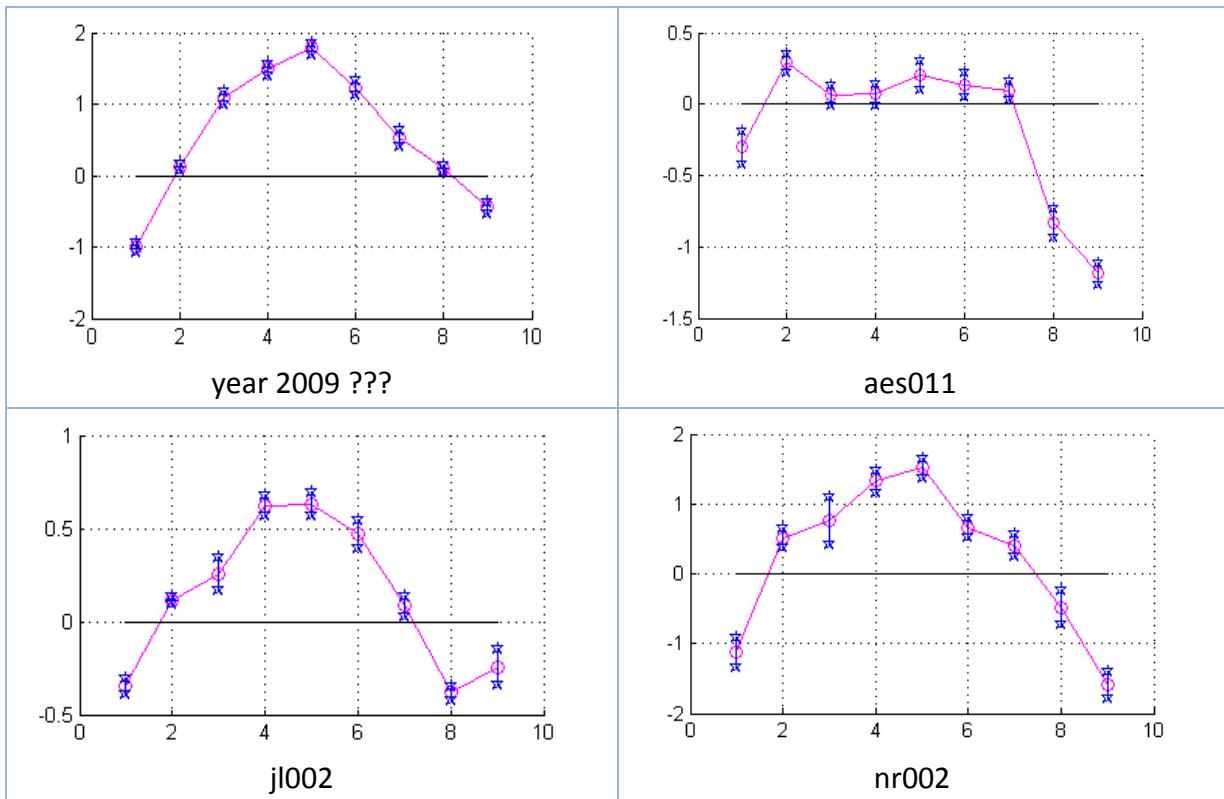


Fig. 14

## 4.2 Collecting focus data

As you have seen, the explored region gradually gets out of focus due to inspection systems design and cavity shape imprecision. The information from the Fig. 12 can be used to calculate how often autofocusing procedure should take place in order to keep the surface in focus with the precision of *effective focus depth* (see *autofocus* section for *effective focus depth*).

It must be noted that two Fermilab inspection systems differ in design. Therefore, the requirements for focusing frequency will be different. More specifically, on the 1<sup>st</sup> system the cavity rotation accounts for changing angle  $\gamma$ , while on the 2<sup>nd</sup> system it is the cylinder with the camera that rotates. That means that on the 2<sup>nd</sup> system a slight cylinder displacement from the cavity axis can dramatically increase the differences of the focal distances. Therefore, a more frequent focus adjustment may be necessary for the 2<sup>nd</sup> system.

Besides changing with the angle  $\gamma$ , the focal distance also differs for different  $z$  mirror angles. This is usually due to the difficulty to adjust the cavity at the center of the equator weld in case the cavity was polished.

On the Fig. 15 you can see the focal distances for the 9<sup>th</sup> equators for different values of  $y$  and  $z$ . Every  $z$  value corresponds to a separate plot (bottom/center/top). The different shape of the plots is due to outliers and the non-uniform lighting conditions, which make different regions of the equator weld be selected for focusing by the program. These plots were analyzed to choose how often it is necessary to perform focusing in order to stay within the *focal depth*.

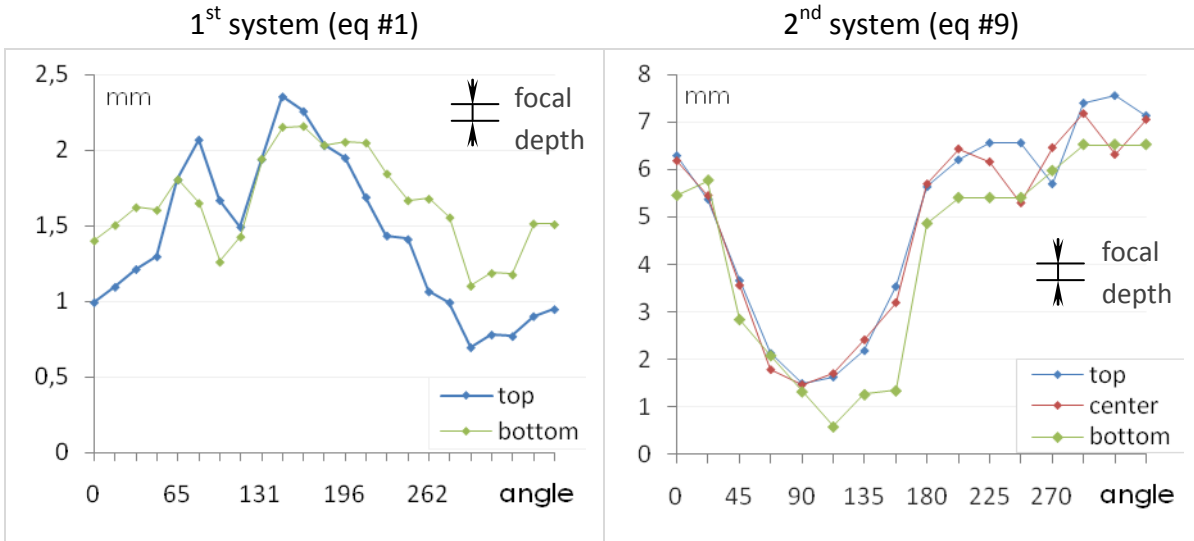


Fig. 15

It is impossible to perform autofocus for every single image, since the procedure takes much time (10-30 sec., depending on the system). We chose to perform autofocus for every value of  $z$  from its range and with a certain preset *period* of  $y$  angle. The focal distances of the angles from between are calculated by the linear interpolation.

We used the following algorithm:

- 1) rotate the cavity from  $y_0$  to  $y_0 + period$
- 2) perform autofocus for every  $z \in [-z_{max}; z_{max}]$ . Write the collected focus information into the array  $F(y; z)$
- 3) use the array to check if the last collected information contained outliers and, if necessary, to restore the correct focus distance values (see below)
- 4) interpolate the array values for  $y \in (y_0; y_0 + period)$ ,  $z \in [-z_{max}; z_{max}]$
- 5) return to  $y = y_0$

### 4.3 Check for outliers

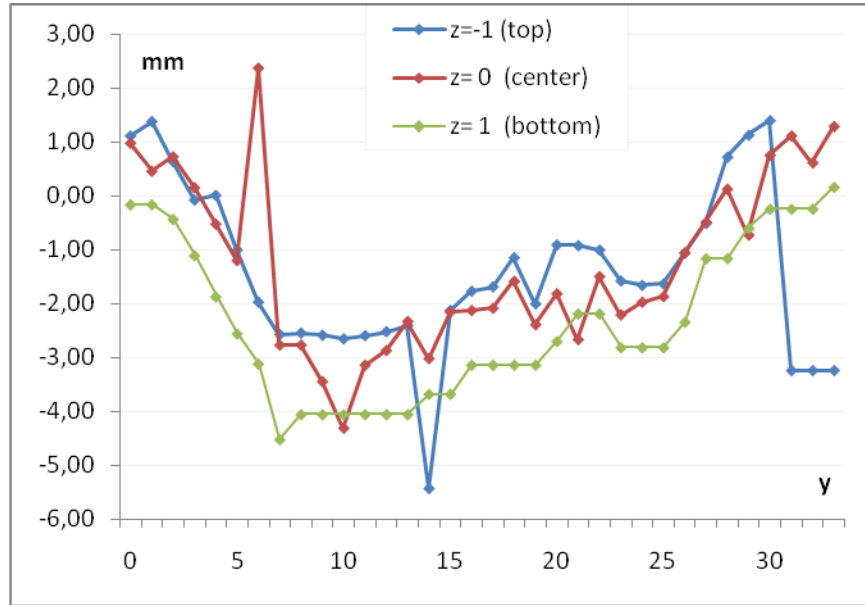


Fig. 16

The autofocus can give a wrong result or fail due to several reasons. Hence, the algorithm above includes a check for outliers, which takes place at step (3). The data just obtained are compared to the whole set of previously collected data.

The inputs of the “check for outliers” algorithm are the array  $F(y; z)$   $y \in [0; y_0]$   $z \in [-z_{\max}; z_{\max}]$  and the last collected data  $f(z) = F(y_0 + period; z)$ , which is actually checked. The output is the binary array  $Outlier(z)$ , which assigns a binary one or zero to every  $z$  from its range.

There may be different criteria for an outlier based on the used information. One approach is to analyze  $f(z)$  for every value of  $z$  separately. For a particular  $z = z_0$  the decision is based only on the sub-array  $F(y; z_0) = F_{z_0}(y)$ . The function  $F_{z_0}(y)$  is extrapolated to predict  $F_{z_0}(y_0 + period) = f^*(z)$ , which is compared to the observed  $f(z)$ . The observed  $f(z)$  can be considered an outlier if, for example,  $|f(z) - f^*(z)|$  exceeds a preset limit. This approach does not make advantage of the fact that the plots for different values of  $z$  have the similar shape [Fig. 16].

Different extrapolation options include using the Kalman filter and the extrapolation based on the linear weighted fitting. The simplest naive version of the

latter is to use only the last obtained value of  $F_z(y)$ :  $f^*(z) = F_z(y_0)$ . Another option is to use three last obtained values of  $F_z(y)$  with different weights:

$$F_z(y_0 + period) = f^*(z) = \text{fitting} \begin{pmatrix} F_z(y_0 - 2 \cdot period), & w=1 \\ F_z(y_0 - period), & w=2 \\ F_z(y_0), & w=3 \end{pmatrix}$$

Kalman filter uses all the given information and generally produces a smoother plot. Two described approaches to fitting are presented in the chart:

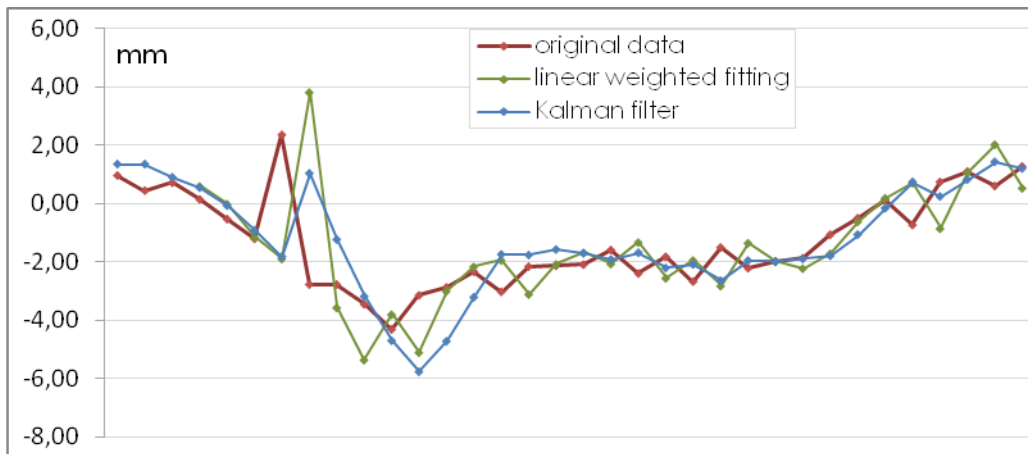


Fig. 17

So far we have been describing the approach based on historical data for every particular  $z$ . Another option is to compare values of  $f(z)$  array if  $z_{\max} > 0$ . If the standard deviation, for example, is more than its preset maximum limit, there is an outlier. Moreover, if  $z_{\max} > 0.5$  ( $num_z > 2$ ) it is possible to track it down. This approach does not take into account the historical data.

The logical “OR” function is used to combine these two criteria:  $f(z)$  is regarded as an outlier if it is considered to be an outlier by any of criteria.

If an outlier is found it has to be replaced with another value. First, we try to repeat autofocusing with another ROI parameter. If the check indicates an outlier one more time,  $f(z)$  value is replaced with  $F(y_0; z)$ . It cannot be replaced with the extrapolated value  $f^*(z)$  because using  $f^*(z)$  several times in a row may lead to creating a positive feedback loop and to regarding all the further observed values as outliers even if they are not [Fig. 18].

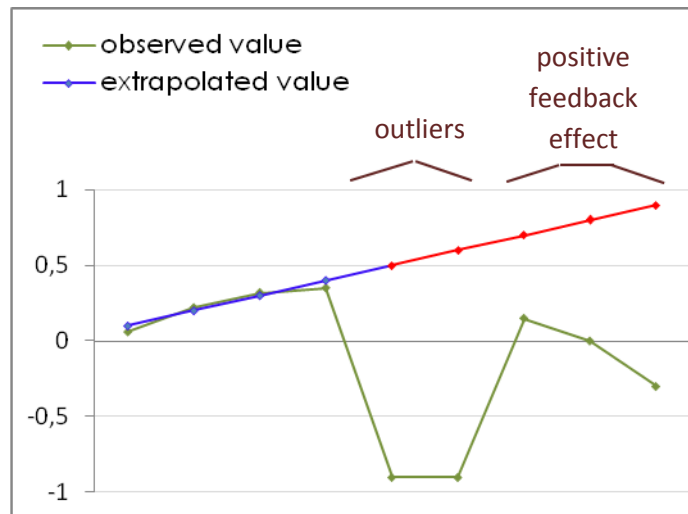


Fig. 18

## CONCLUSION

This paper presents the problems of developing the software for the optical inspection systems of SRF cavities and the methods to solve them. The stress was made on the issues of autofocusing. They include the components of the autofocus itself and the methods to use it most effectively.

Based on this paper a software developer may use the following steps as guidance:

1. Select a metrics for autofocusing
2. Select an algorithm to choose the region on the surface to focus on
3. Select a method to achieve focused position
4. Choose how often to perform autofocusing
5. Select a method to manage autofocus mistakes (outliers)

The presented methods can also be used to study the imperfections of the cavity shape.

## References

- [1] Y. Sun, S. Duthaler, B. J. Nelson, "Autofocusing Algorithm Selection in Computer Microscopy," *IEEE/RSJ International Conference on Intelligent Robots and Systems*, 2005
- [2] K. Ooi, K. Izumi, M. Nozaki, I. Takeda, "An Advanced Auto-Focus System for Video Camera Using Quasi Condition Reasoning," *Consumer Electronics, 1990. ICCE 90. IEEE*, 1990
- [3] J. He, R. Zhou, Z. Hong, "Modified fast climbing search auto-focus algorithm with adaptive step size searching technique for digital camera," *Consumer Electronics, IEEE Transactions on*, 2003
- [4] E Toropov, E. Tripodi, "Optical inspection of SRF cavities," *Fermi National Accelerator Laboratory report*, 2009, pp 19-24